J Biomol NMR (2013) 55:157–166
DOI 10.1007/s10858-012-9697-3

ARTICLE

A systematic study of labelling an α-helix in a protein with a lanthanide using IDA-SH or NTA-SH tags

Hiromasa Yagi · Ansis Maleckis · Gottfried Otting

Received: 9 October 2012 / Accepted: 15 December 2012 / Published online: 22 December 2012

Abstract The previously published IDA-SH and NTA-SH tags are small synthetic lanthanide-binding tags derived from cysteine, which afford site-specific lanthanide labelling by disulfide-bond formation with a cysteine residue of the target protein. Following attachment to a single cysteine in an α-helix, sizeable pseudocontact shifts (PCS) can be observed, if the lanthanide is immobilized by additional coordination to a negatively charged amino-acid side chain that is located in a neighboring turn of the helix. To identify the best labelling strategy for PCS measurements, we performed a systematic study, where IDA-SH or NTA-SH tags were ligated to a cysteine residue in position i of an α-helix, and aspartate or glutamate residues were placed in the positions $i - 4$ or $i + 4$. The largest anisotropy components of the magnetic susceptibility tensor were observed for an NTA-SH tag in position i with a glutamate residue in position $i - 4$. While the NTA-SH tag produced sizeable PCSs regardless of the presence of nearby carboxyl groups of the protein, the IDA-SH tag generated a good lanthanide binding site only if an aspartate was placed in position $i + 4$. The findings provide a firm basis for the design of site-directed mutants that are suitable for the reliable generation of PCSs in proteins with paramagnetic lanthanides.

Keywords Lanthanide tag · IDA-SH tag · NTA-SH tag · NMR spectroscopy · Pseudocontact shifts · ERp29

Electronic supplementary material The online version of this article (doi:10.1007/s10858-012-9697-3) contains supplementary material, which is available to authorized users.

H. Yagi · A. Maleckis · G. Otting (✉)
Research School of Chemistry, Australian National University, Canberra, ACT 0200, Australia
e-mail: go@rsc.anu.edu.au

A. Maleckis
Latvian Institute of Organic Synthesis, Riga 1006, Latvia

Introduction

Paramagnetic lanthanide ions offer unique opportunities for structural biology by NMR spectroscopy. Among the paramagnetic effects produced by lanthanide ions, pseudocontact shifts (PCS) stand out for their ease of measurement in NMR spectra and the fact that they can be observed over a large distance range (about 10–40 Å) from the paramagnetic centre (Allegrozzi et al. 2000; Pintacuda et al. 2007; Otting 2008, 2010; Koehler and Meiler 2011). PCSs thus present highly useful long-range structural restraints for protein structure refinement (Allegrozzi et al. 2000; Banci et al. 2004; Knight et al. 2012) and rapid structure analysis of biomolecular assemblies (Pintacuda et al. 2006; John et al. 2006; Keizers et al. 2010; Saio et al. 2010, 2011). They have also been used for resonance assignments of protein NMR spectra by reference to the three-dimensional (3D) structure of the protein (Schmitz et al. 2006; de la Cruz et al. 2011) and present powerful restraints for the identification of the three-dimensional (3D) fold of proteins (Schmitz et al. 2012).

The PCS $\Delta\delta^{PCS}$ of a nuclear spin depends on its polar coordinates r, θ and φ with respect to the principal axes of the $\Delta\chi$ tensor

$$\Delta\delta^{PCS} = \frac{1}{12\pi r^3}\left[\Delta\chi_{ax}\left(3\cos^2\theta - 1\right) + \frac{3}{2}\Delta\chi_{rh}\sin^2\theta\cos 2\varphi\right] \quad (1)$$

where $\Delta\chi_{ax}$ and $\Delta\chi_{rh}$ denote, respectively, the axial and rhombic components of the magnetic susceptibility tensor χ (Bertini et al. 2002), and were the $\Delta\chi$ tensor is defined as

the χ tensor minus its isotropic component, in analogy to the definition of the alignment tensor (Kramer et al. 2004). To decode the structural information contained in the PCSs, the $\Delta\chi$ tensor of the lanthanide must be determined, including the position of the lanthanide and the orientation of the principal coordinate system of the $\Delta\chi$ tensor relative to the protein. Fitting the parameters of the $\Delta\chi$ tensor to the structure of the protein involves minimizing the mean square deviation between the experimental and back-calculated PCSs.

In practice, the experimental PCSs are all measured for protein resonances, because large paramagnetic relaxation enhancements (PRE) prevail in the immediate vicinity of any paramagnetic metal ion, broadening NMR signals beyond detection. Fitting the $\Delta\chi$ tensor to the PCSs of the protein, however, becomes problematic if the metal ion is attached to the protein by a flexible tether: if the metal ion assumes multiple positions relative to the protein, the fitted $\Delta\chi$ tensor presents a single effective average tensor which cannot accurately describe the ensemble of $\Delta\chi$ tensors produced by the different positions and orientations of the lanthanide. As PCSs can assume both positive and negative values (Eq. 1), an effective $\Delta\chi$ tensor tends to be smaller than the true tensor associated with the tag and can quite easily average to zero. The best lanthanide-labelling strategies thus achieve high immobilization of the lanthanide ion relative to the protein.

Except for metallo-proteins that allow the substitution of a metal ion by a lanthanide, proteins rarely contain natural lanthanide binding sites. Therefore, a large variety of lanthanide-binding tags (LBT) have been developed for site-specific labelling of proteins with a lanthanide ion (Ma and Opella 2000; Dvoretsky et al. 2002; Wöhnert et al. 2003; Ikegami et al. 2004; Häussinger et al. 2009; Rodriguez-Castañeda et al. 2006; Su et al. 2009; Su and Otting 2010; Jia et al. 2011; Graham et al. 2011; Peters et al. 2011; Li et al. 2012). High immobilization of the LBT can be achieved by a bulky LBT that is restricted in its motions by steric interactions (Su et al. 2006; Martin et al. 2007; Graham et al. 2011), double-arm attachment (Prudêncio et al. 2004; Vlasie et al. 2007; Keizers et al. 2007, 2008; Saio et al. 2009; Liu et al. 2012), insertion into the loop region of the target protein (Barthelmes et al. 2011) or by additional coordination of the lanthanide ion by the carboxyl group of an amino-acid side chain of the protein (Su et al. 2008; Man et al. 2010; Jia et al. 2011; Swarbrick et al. 2011a).

Particularly attractive tags are presented by the small molecules shown in Fig. 1. The tags are hybrids of the tridentate chelator iminodiacetic acid (IDA) and cysteine (in the following referred to as IDA-SH), or of the tetradentate chelator nitrilotriacetic acid (NTA) and cysteine (in the following referred to as NTA-SH). Both tags can easily

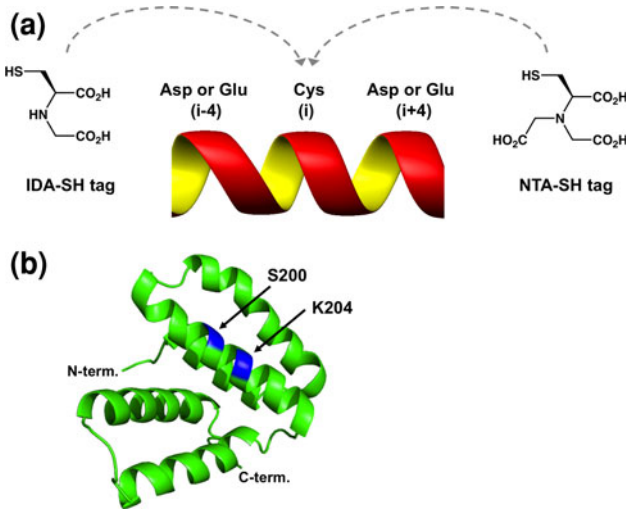

Fig. 1 Lanthanide tagging strategy investigated in the present work. **a** Chemical structures of the IDA-SH and NTA-SH tags used and helix model indicating the positions $i - 4$, i, and $i + 4$. **b** Crystal structure of ERp29-C (residues 155-256, PDB ID 2QC7) (Barak et al. 2009). The residues 200 and 204 are highlighted in *blue*

be synthesized from L-cysteine. They can be attached to cysteine residues of the protein by formation of a disulfide bond following activation of the protein with Ellman's reagent (5,5′-dithiobis-(2-nitrobenzoic acid), DTNB; Su et al. 2006). Bound paramagnetic lanthanide ions produce single sets of peaks in the protein NMR spectra as expected for single conformational species. As the IDA-SH and NTA-SH tags are only tridentate and tetradentate, respectively, the remaining coordination sites of the lanthanide ion can be filled by hydration water or by carboxyl groups of the protein.

In an elegant demonstration of the IDA-SH tag, Swarbrick et al. (2011a) showed that an IDA-SH tag that is attached to a cysteine residue in position i of an α-helix can combine with the carboxyl group of an aspartic acid residue in position $i + 4$ to coordinate a lanthanide ion with an affinity that allows the observation of exchange cross-peaks between molecules coordinated with paramagnetic and diamagnetic ions. The exchange cross-peaks greatly facilitate the assignment of the cross-peaks of the paramagnetic species (John et al. 2007). It has also been shown that a pair of NTA-SH tags attached to cysteines in positions i and $i + 4$ of an α-helix can act together to bind a single lanthanide ion tightly and rigidly, leading to significant PCSs and RDCs (Swarbrick et al. 2011b). As a drawback, this scheme requires the simultaneous presence of two solvent-exposed cysteine residues at positions i and $i + 4$ of an α-helix.

To explore the general applicability of the IDA-SH and NTA-SH tags for lanthanide labelling, we performed a systematic study of the potential of negatively charged

amino-acid side chains in neighboring turns of an α-helix to immobilize a lanthanide ion that is coordinated to either an IDA-SH or an NTA-SH tag attached to a cysteine residue in position *i* of the same helix. As a model system we used the C-terminal domain of the rat endoplasmic reticulum 29 kDa protein (ERp29-C, residues 155–260; Liepinsh et al. 2001). This domain comprises five α-helices. The naturally occurring cysteine residue, Cys157, was mutated to serine and either Ser200 or Lys204 in helix 3 were mutated to cysteine. With a cysteine residue in position 200 (position *i*), samples were made with Lys204 (position $i + 4$) mutated to aspartate or glutamate. With a cysteine residue in position 204 (position *i*), samples were made with Ser200 (position $i - 4$) mutated to aspartate or glutamate (Fig. 1). In addition, control experiments were performed without the additional aspartate and glutamate mutations. The metal positions were determined by fitting $\Delta\chi$ tensors to the crystal structure of the homologous human protein (Barak et al. 2009), using PCSs observed with different lanthanides. The results provide a firm basis for the design of lanthanide binding sites that are likely to immobilize the metal ion and produce large PCSs.

Materials and methods

Sample preparation

Detailed protocols for the synthesis of the IDA-SH and NTA-SH tags are provided in the Supporting Information.

The mutants S200C/C157S, S200C/K204D/C157S, S200C/K204E/C157S, S200D/K204C/C157S, S200E/K204C/C157S and K204C/C157S were introduced into ERp29-C. Each construct contained a His_6-tag at the C-terminus. The proteins were expressed by the plasmid pETMCSI (Neylon et al. 2000) under control of the T7-promoter. Uniformly ^{15}N- or $^{13}C/^{15}N$-labelled samples were expressed in *Escherichia coli* Rosetta (λDE3)/pRARE cells. For protein production, cells were grown overnight in 10 mL of LB medium. This pre-culture was used to inoculate 1 L of minimal medium containing $^{15}NH_4Cl$ as the sole nitrogen source or [U–^{13}C] glucose and $^{15}NH_4Cl$ as the sole carbon and nitrogen sources. The cells were grown at 37 °C. Protein expression was induced by adding 1 mM isopropyl β-D-1-thiogalactopyranoside (IPTG) at $OD_{600} = 0.6$ and the cells were harvested 6 h after induction. Each protein sample was purified by a HisTrap HP column (GE Healthcare, 5 mL). The ligation of the ERp29-C mutants with the NTA-SH and IDA-SH tags followed the previously published protocol (Swarbrick et al. 2011a, b), except that 20 mM Tris·HCl, pH 7.6, was used as the ligation buffer.

NMR spectroscopy

All NMR spectra were recorded using 0.2–0.4 mM solutions of the ERp29-C mutants in 20 mM MES (pH 4.9) buffer at 31 °C on a Bruker Avance 800 MHz NMR spectrometer with a TCI cryoprobe. PCSs were measured as the difference in ^1H chemical shift observed in ^{15}N-HSQC spectra of samples with a paramagnetic lanthanide (Tm^{3+} and Yb^{3+}) minus the corresponding chemical shifts with a diamagnetic metal (Y^{3+}). Each metal ion was supplied to the tagged protein in equimolar ratio. For all triple mutants, the assignments of the paramagnetic peaks obtained with Tm^{3+} were verified by 3D HNCO spectra of the $^{13}C/^{15}N$-labelled proteins.

Tensor fitting

$\Delta\chi$ tensors were fitted to the crystal structure of the C-terminal domain of human ERp29 (PDB ID 2QC7) (Barak et al. 2009) using all available experimental PCSs of the amide protons (Table S1). Fits were performed with the program PyParaTools (M. Stanton-Cook and T. Huber, unpublished results) as described previously (Graham et al. 2011; Swarbrick et al. 2011b; de la Cruz et al. 2011), using rotamer libraries of the tags to identify all possible tag conformations and metal positions while keeping the protein coordinates fixed. In a second step, $\Delta\chi$ tensors were fitted to every rotamer model, simultaneously using the PCS data obtained with Tm^{3+} and Yb^{3+}. The rotamer with the smallest root-mean-square deviation between experimental and back-calculated PCSs was identified. Corrections to account for residual anisotropic chemical shifts (John et al. 2005) made no significant difference to the tensor parameters. The metal position found was checked for the possibility of additional coordination by carboxyl groups of aspartate or glutamate. Different side chain rotamers of aspartate and glutamate were explored by interactive use of PyMOL (De Lano 2002), which also checked for van der Waals clashes. For comparison, $\Delta\chi$-tensor fits were also performed with the program Numbat (Schmitz et al. 2008).

Results

Protein samples

The structure of ERp29-C comprises five α-helices (Fig. 1b; Liepinsh et al. 2001). As wild-type ERp29-C contains a single cysteine in position 157, this residue was mutated to serine in all constructs. To study the effect of negatively charged amino acids on a lanthanide coordinated to an IDA-SH or NTA-SH tag while minimising

specific influences from the protein environment, the additional mutations were restricted to residues 200 and 204 on the solvent-exposed face of the third α-helix (Fig. 1b). The position *i* was defined as the position of the cysteine residue that was ligated with the IDA-SH or NTA-SH tag. The effects of aspartate or glutamate in position $i + 4$ were tested with the mutants S200C/K204D and S200C/K204E, whereas the effects of aspartate or glutamate in position $i - 4$ were tested with the mutants S200D/K204C and S200E/K204C. In addition, the mutants S200C and K204C were also made as controls. These mutants contained no negatively charged residue in the positions $i + 4$ or $i - 4$. In the following, the double and triple mutants of ERp29-C (C157S/S200C, C157S/K204C, C157S/S200C/K204D, C157S/S200C/K204E, C157S/S200D/K204C and C157S/S200E/K204C) are for simplicity referred to as the mutants C200, C204, C200/D204, C200/E204, D200/C204 and E200/C204, respectively. All proteins were soluble and the expression yields were about 10–15 mg/L M9 medium. Typical ligation yields with the IDA-SH and NTA-SH tags were 70 %. None of the samples precipitated during the NMR measurements with lanthanides.

Δχ tensor determinations

The Δχ tensors were determined from the PCSs observed for backbone amide protons. The assignments of the diamagnetic references, i.e. the complexes formed with Y^{3+}, were straightforward to establish by comparison with the published assignments of the wild-type protein (Liepinsh et al. 2001). Attempts to measure N_z-exchange spectra (John et al. 2007) with the ERp29-C C200/D204 mutant with attached IDA-SH tag yielded only very weak cross-peaks, so that this experiment could not be used to assign the ^{15}N-HSQC cross-peaks in the paramagnetic state. Instead, we assigned the peaks in the paramagnetic NMR spectra by using two different paramagnetic lanthanide ions, Tm^{3+} and Yb^{3+}, that shift the cross-peaks in the ^{15}N-HSQC spectrum in the same direction but by different amounts. The assignments of the spectra recorded with Tm^{3+} were confirmed by 3D HNCO spectra, where each cross-peak must display a similar PCS in the ^{13}C dimension as in the ^{15}N and ^{1}H dimensions, since the three correlated spins are close to each other compared with their distance from the paramagnetic centre. At least 28 PCSs were measured for each metal ion and mutant (Tables S1–S7) and the Δχ-tensor fits were performed for the Tm^{3+} and Yb^{3+} data sets simultaneously, using a common metal position. To ensure agreement with the covalent structure of the tagged protein, the fits selected the metal position from a library of tag conformations. The tag rotamer producing the best-fitting Δχ tensor was used to check for the possibility of additional coordination of the lanthanide ion by neighboring aspartate or glutamate residues, allowing all conceivable staggered rotamers.

For all mutants and tags, the best fits resulted in small *Q*-factor values (Table 2) and close correlations between the back-calculated and observed PCSs (Figure S6), indicating that any tag motions are sufficiently small in amplitude to allow interpretation of the PCSs by a single effective Δχ tensor. Restraining the metal coordinates by the covalent structure of the tag did not significantly affect the Δχ-tensor fits. This was evidenced by the similarity of the Δχ-tensors obtained by fitting with and without restraints on the metal position, where no $\Delta\chi_{ax}$ or $\Delta\chi_{rh}$ component varied by more than 0.4×10^{-32} m^3 (Tables 2 and S8). Furthermore, the unrestrained fits displaced the metal ion positions by no more than 0.7 Å, except for the C200 mutant with NTA-SH tag, for which significantly increased mobility of the tag is indicated by small Δχ tensors (Table S8). This result attests to the reliability of the Δχ tensors and metal positions derived from the fits.

IDA-SH tag

In the case of the IDA-SH tag, only the C200/D204 mutant lead to sizeable PCSs with the lanthanide ions Tm^{3+} and Yb^{3+} (Table 1; Fig. 2; Figures S1–S5). Large PCSs were expected based on the data published for human ubiquitin, where the IDA-SH tag was attached to a cysteine in position 28 in the vicinity of Asp32 in the same α-helix (Swarbrick et al. 2011a). Unexpectedly, none of the other ERp29-C mutants showed evidence of site-specific lanthanide binding, although some ^{15}N-HSQC cross-peaks shifted slightly upon the addition of lanthanide ions (Figures S1–S5). These shifts, however, seemed to arise from non-specific binding of the lanthanides. Firstly, they increased with increasing amounts of lanthanide beyond the 1:1 lanthanide-to-protein ratio, which would be expected to saturate the tag. Secondly, the shifting peaks belonged to residues 166–175, 212–219, 234–239 and 252–256, which are located in different solvent-exposed regions of the protein. Their NMR resonances also shifted in the absence of any lanthanide tags.

The Δχ tensors determined for the C200/D204 mutant positioned the metal ion in close proximity of the side chain of Asp204 as expected. Table 2 shows the tensor parameters of the overall best fit. The axial components of the Δχ tensors are quite large (within 30 % of those determined for ubiquitin Ala28Cys with IDA-SH tag; Swarbrick et al. 2011a), indicating that the metal ion is well immobilized relative to the protein. The corresponding tag rotamer is displayed in Fig. 3. To build this model, residue 204 was mutated to aspartate and its side-chain orientations were optimized to approach the lanthanide ion

Table 1 Site-specific lanthanide binding to different ERp29-C mutants with IDA-SH or NTA-SH tags

	$i-4=$ D D200/C204	$i-4=$ E E200/C204	Control C204	$i+4=$ D C200/D204	$i+4=$ E C200/E204	Control C200
IDA-SH	No	No	No	Yes	No	No
NTA-SH	Yes	Yes	Yes	Yes	Yes	Yes

All ERp29-C constructs contained the mutation Cys157Ser. In the wild-type protein, the residues at positions 200 and 204 are serine and lysine, respectively. "Yes" means the observation of reasonably large PCSs that can be interpreted by a single $\Delta\chi$ tensor. "No" means the observation of only small PCSs that increased with increasing lanthanide concentration beyond the 1:1 lanthanide-to-protein ratio, indicating non-specific binding of the lanthanide to the protein rather than to the tag

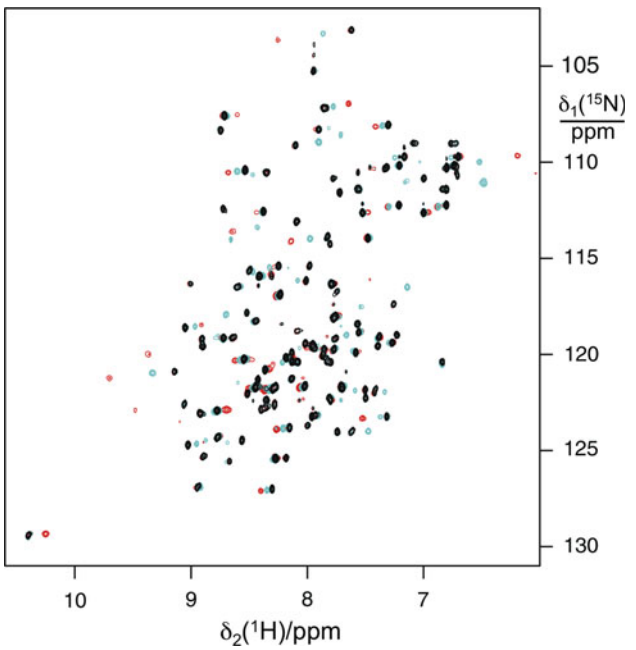

Fig. 2 Superimposition of ^{15}N-HSQC spectra of the uniformly ^{15}N-labelled C200/D204 mutant with IDA-SH tag loaded with Y^{3+} (*black*), Yb^{3+} (*cyan*), or Tm^{3+} (*red*). The spectra were recorded at 31 °C and pH 4.9 at a ^{1}H NMR frequency of 800 MHz. Some of the cross-peaks in the spectrum with Y^{3+} have no counterparts in the spectra with Yb^{3+} or Tm^{3+} due to relaxation enhancements in the vicinity of the paramagnetic lanthanide ions

without van der Waals clashes. This brings the side-chain carboxyl group of Asp204 to within 2.0 Å of the lanthanide ion. The combined results strongly suggest that Asp204 assists the IDA-SH tag in coordinating the lanthanide ion.

NTA-SH tag

To our surprise, Tm^{3+} and Yb^{3+} produced sizeable PCSs for all cysteine mutants of ERp29-C that had been ligated with the NTA-SH tag, even for the control mutants that contained no negatively charged residues in the helix turns neighboring the ligation site (Table 1; Fig. 4). This result illustrates the significantly higher binding affinity of the NTA-SH tag for lanthanide ions compared with the IDA-SH tag. Interestingly, however, the $\Delta\chi$ tensors obtained varied significantly in magnitude and orientation between all six mutants (Table 2), which is also apparent from the different PCSs observed (Fig. 4). This shows that the presence of neighboring negatively charged residues matters, by changing the ligand field of the lanthanide ion, by reducing the residual mobility of the tag or both.

A plausible interpretation of the variation in $\Delta\chi$-tensor magnitudes is obtained by assuming that the different $\Delta\chi$-tensor magnitudes observed in the different mutants primarily reflect different degrees of residual tag mobility.

Table 2 $\Delta\chi$ tensor parameters of ERp29-C mutants with IDA-SH and NTA-SH tags

	Ln^{3+}	$\Delta\chi_{ax}$	$\Delta\chi_{rh}$	Q	α	β	γ
With IDA-SH tag							
C200/D204	Tm^{3+}	9.8 (0.4)	4.9 (0.7)	0.03	30	173	136
	Yb^{3+}	4.8 (0.1)	1.9 (0.2)	0.02	46	170	110
with NTA-SH tag							
D200/C204	Tm^{3+}	6.0 (0.2)	3.4 (0.2)	0.03	58	45	14
	Yb^{3+}	2.2 (0.1)	1.4 (0.1)	0.01	59	59	12
E200/C204	Tm^{3+}	13.0 (0.2)	8.5 (0.4)	0.02	74	35	21
	Yb^{3+}	4.2 (0.1)	2.6 (0.1)	0.01	56	36	35
C204	Tm^{3+}	6.3 (0.4)	1.6 (0.3)	0.02	123	137	2
	Yb^{3+}	1.9 (0.1)	0.5 (0.2)	0.02	123	134	1
C200/D204	Tm^{3+}	6.6 (0.1)	4.2 (0.2)	0.03	133	76	5
	Yb^{3+}	2.4 (0.1)	1.3 (0.1)	0.02	135	81	12
C200/E204	Tm^{3+}	8.2 (0.2)	2.7 (0.1)	0.01	161	50	130
	Yb^{3+}	2.9 (0.2)	1.6 (0.1)	0.03	149	47	125
C200	Tm^{3+}	4.2 (0.1)	0.4 (0.4)	0.02	61	21	138
	Yb^{3+}	1.1 (0.1)	0.3 (0.2)	0.02	68	25	143

The axial and rhombic components of the $\Delta\chi$ tensors are given in 10^{-32} m^3 and the Euler angles in degrees, using the zyz convention and unique tensor representation (Schmitz et al. 2008). The $\Delta\chi$ tensors of the table report the parameters of the overall best fit, using the PCSs of Tables S1–S7 to fit tensors to the crystal structure of ERp29-C (PDB ID 2QC7) (Barak et al. 2009) onto which a library of modeled tag conformations was crafted. Error estimates (in brackets) were determined from fits obtained by using the same metal position while randomly omitting 10 % of the PCS data. Quality factors (Q) were calculated as the root-mean-square deviation between experimental and back-calculated PCSs divided by the root-mean-square of the experimental PCSs. The final fits used corrections to account for residual anisotropic chemical shifts (John et al. 2005)

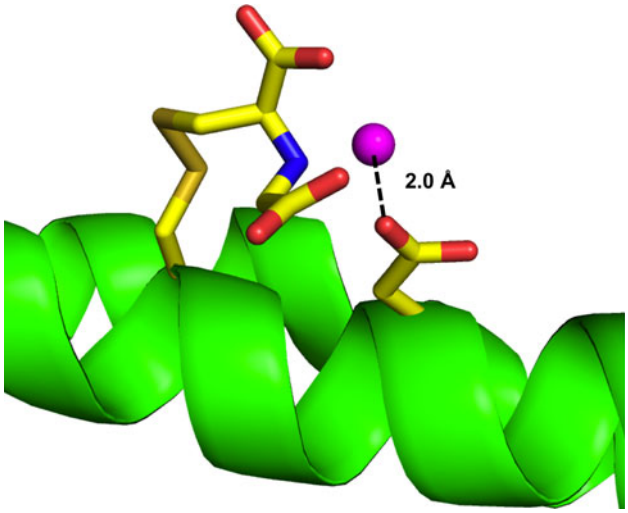

Fig. 3 Model of the lanthanide binding site produced by the IDA-SH tag attached to the C200/D204 mutant. The model was selected from a rotamer library of the IDA-SH tag by the criterion of producing the best $\Delta\chi$-tensor fit. The IDA-SH tag and the side chain of Asp204 are shown as stick models. The side-chain dihedral angles of Asp204 were manually adjusted to bring the carboxyl group into close proximity of the lanthanide ion without introducing van der Waals clashes. C, N, O and S atoms are colored *yellow*, *blue*, *red* and *orange*, respectively. The position of the metal ion is shown as a *magenta sphere*

For example, the $\Delta\chi$ tensors were particularly small for the C200 and C204 mutants, as expected for an increased degree of averaging between different tensor orientations relative to the protein. Conversely, the presence of aspartate and glutamate residues consistently generated larger $\Delta\chi$-tensor magnitudes, suggesting that they assist in immobilizing the lanthanide ion at least to some degree. This interpretation is supported by the position of the metal ions determined by the $\Delta\chi$-tensor fits.

Figure 5 displays those rotamers of the NTA-SH tag moiety in the six different ERp29-C mutants that yielded the best $\Delta\chi$-tensor fits. In addition, the models display side-chain conformations of the aspartate and glutamate residues located in neighboring helix turns, which were interactively modeled to project their carboxyl group towards the metal ion.

Among the mutants with the NTA-SH tag attached at position 204, the E200/C204 mutant showed the largest $\Delta\chi$ values. Coordination of the lanthanide by the side-chain carboxyl group of the glutamate residue in position $i - 4$ is clearly suggested by the location of the metal ion between residues 200 and 204 (Fig. 5a).

In the mutant D200/C204, Glu200 is replaced by an aspartate. The $\Delta\chi$-tensor values are smaller (Table 2) and the side chain of Asp200 cannot be brought into the same close proximity of the metal ion as in the case of the E200/C204 mutant (Fig. 5b), suggesting greater residual mobility of the metal ion. In fact, the $\Delta\chi$-tensor values of the D200/C204 mutant are similarly small as in the control mutant C204, which has no negatively charged side chain in proximity of the NTA-SH tag. Nonetheless, the presence of Asp200 influences the metal position, which is between residues 200 and 204 in the D200/C204 mutant but on the opposite side of the NTA-SH tag in the control mutant C204 (Fig. 5c).

Among the mutants carrying the NTA-SH tag in position 200, the C200/E204 mutant produced the largest $\Delta\chi$ values. They were, however, consistently smaller than for the E200/C204 mutant and also smaller than for the C200/D204 mutant with IDA-SH tag (Table 2). The C200/E204 mutant with NTA-SH tag places the lanthanide between residues 200 and 204, and the side chain of E204 can be rotated to approach the lanthanide for additional coordination. Indeed, the control mutant C200 positions the lanthanide on the other side of the NTA-SH tag (Fig. 5d, f), confirming that Glu204 assists the immobilization of the lanthanide ion. Interestingly, the C200/D204 mutant did not produce particularly large $\Delta\chi$ tensors with the NTA-SH tag, in stark contrast to the same mutant with the IDA-SH tag. With the NTA-SH tag, the C200/D204 mutant also showed no evidence of Asp204 coordinating the lanthanide ion, although the metal was positioned closer to residue 204 than in the C200 control mutant (Fig. 5e, f) and the $\Delta\chi$ tensors were somewhat larger, too (Table 2).

Discussion

The present work produced some unexpected results. For example, the C200/D204 mutant was the only mutant that produced good $\Delta\chi$ tensors with the IDA-SH tag. This may be attributed to the much weaker lanthanide affinity of the IDA-SH tag compared with the NTA-SH tag, requiring additional coordination of the lanthanide by a carboxyl group from the protein to produce a good lanthanide binding site. Apparently, however, the IDA-SH tag forms good lanthanide binding sites only if all aspects are right for lanthanide coordination. In contrast, all mutants delivered sizeable PCSs with the NTA-SH tag, indicating that the failure of the IDA-SH tag to produce good lanthanide binding sites in most cases is a consequence of its intrinsically weak affinity for lanthanides.

The magnitudes of the $\Delta\chi$ tensors are sensitive to the coordination geometry of the lanthanide ions. Furthermore, the tensors determined in the present work are effective $\Delta\chi$ tensors that depend on the precise movement of the metal with respect to the protein. Nonetheless, a consistent interpretation of the data in the present work can be gained by the hypothesis that the variable magnitudes of the $\Delta\chi$ tensors mostly reflect different degrees of PCS averaging arising from different extents of residual tag mobility. For

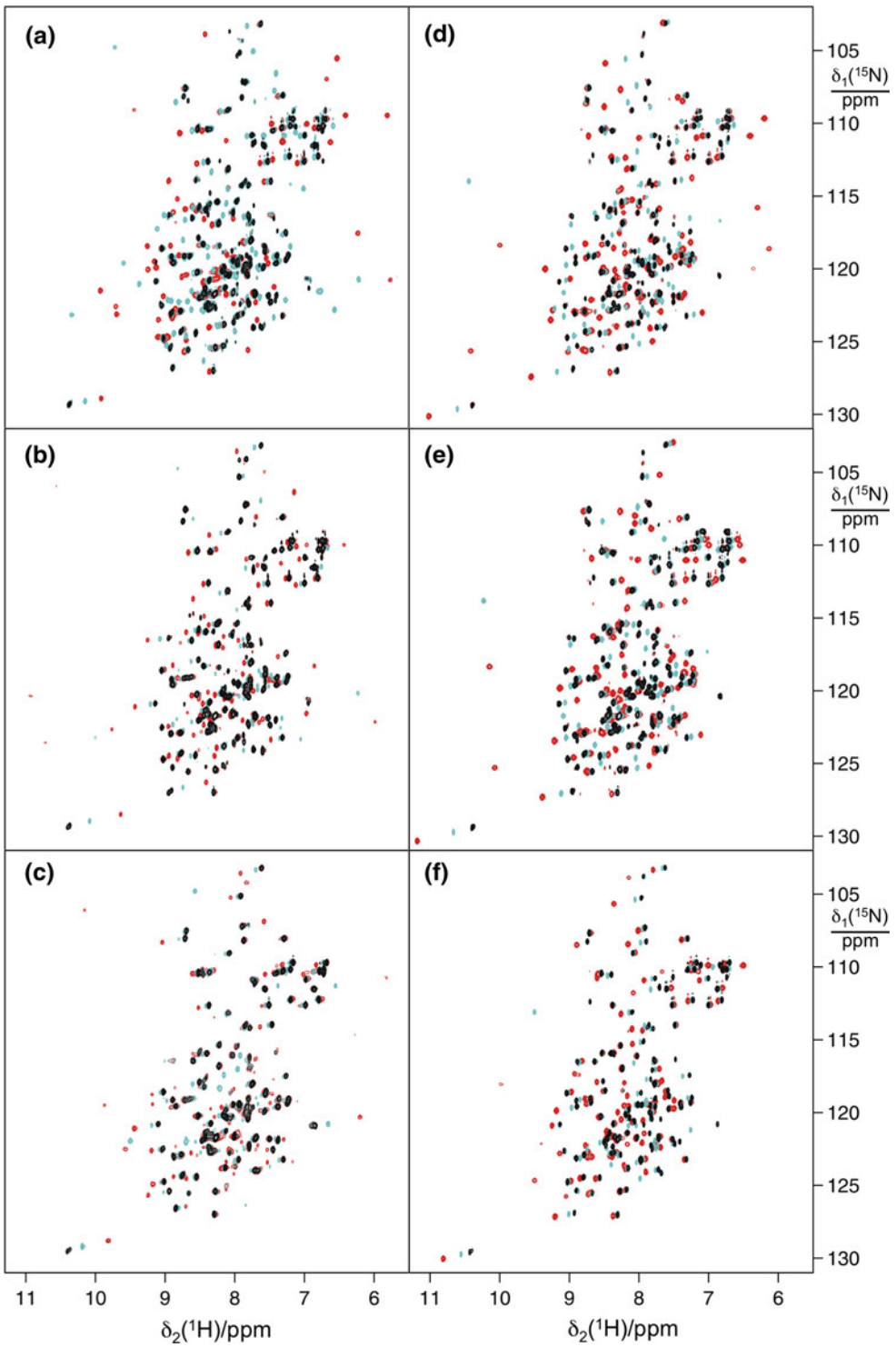

Fig. 4 Superimposition of ^{15}N-HSQC spectra of uniformly ^{15}N-labelled ERp29-C mutants with NTA-SH tag loaded with Y^{3+} (*black*), Yb^{3+} (*cyan*) or Tm^{3+} (*red*). All spectra were recorded at 31 °C and pH 4.9 at a ^{1}H NMR frequency of 800 MHz. The mutants are **a** E200/C204, **b** D200/C204, **c** C204, **d** C200/E204, **e** C200/D204 and **f** C200

example, the mutants E200/C204 and C200/E204 produced the largest $\Delta\chi$ tensors and seem to achieve this by additional coordination of the lanthanide by the carboxyl group of the glutamate residue. Steric hindrance by the larger NTA-SH tag that prevents good lanthanide coordination by aspartates may explain why the C200/D204 mutant gave poorer PCSs with the NTA-SH tag than with the IDA-SH tag. It is worth noting that the largest $\Delta\chi$ tensor was obtained for the E200/C204 mutant with NTA-SH tag, suggesting similarly good immobilization of the lanthanide as in the C200/D204 mutant with IDA-SH tag. Measurements of the residual dipolar couplings (RDC) between amide nitrogens and amide protons, $^{1}D_{NH}$, for the E200/C204 mutant with NTA-SH tag and Tm^{3+} on a 800 MHz

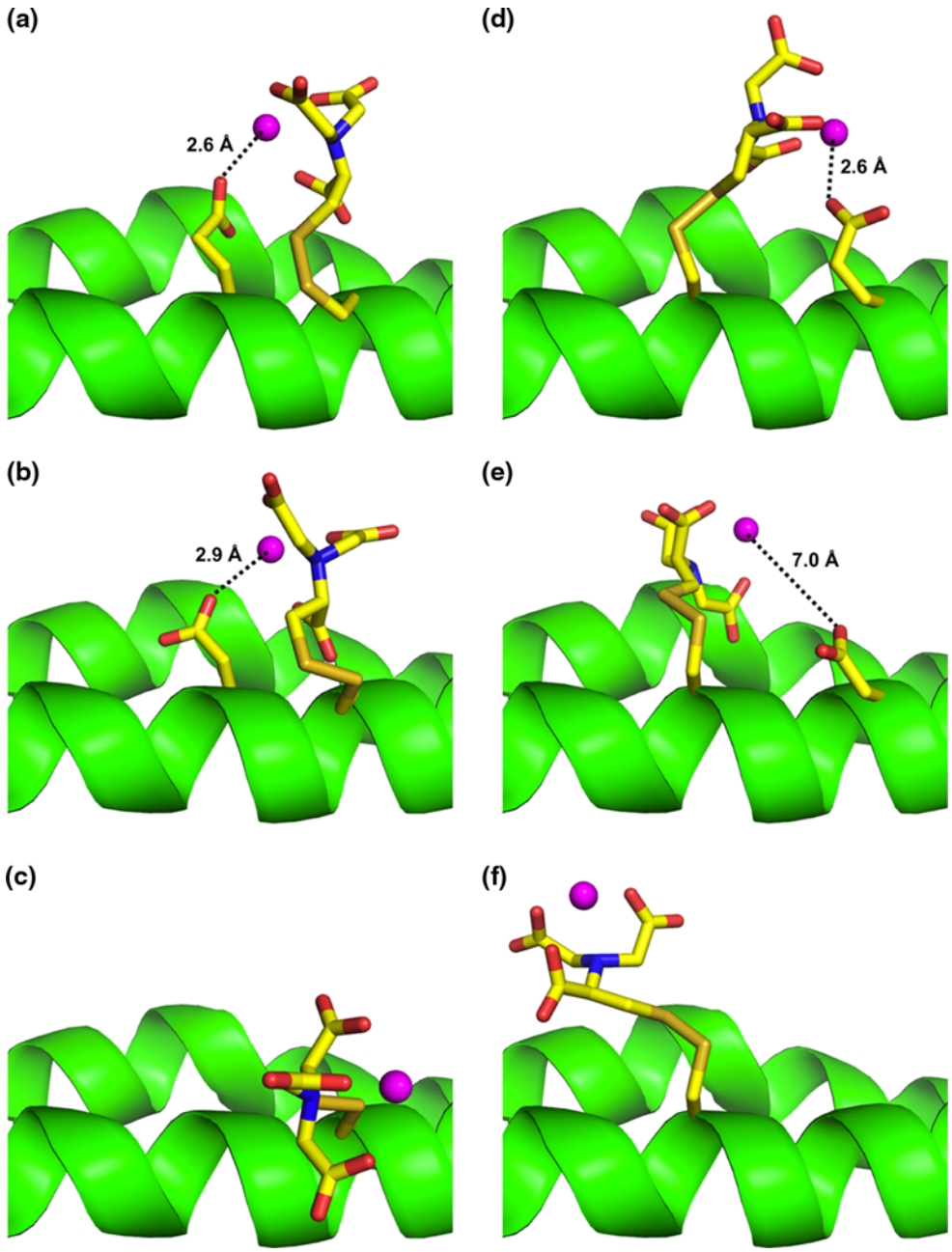

Fig. 5 Models of the lanthanide binding sites produced by the NTA-SH tag attached to the ERp29-C mutants. The NTA-SH tag and the side chains of residues in the positions $i - 4$ and $i + 4$ are shown as stick models. C, N, O and S atoms are colored *yellow*, *blue*, *red* and *orange*, respectively. The position of the metal ion is shown as a magenta sphere. For each mutant, the model shown was selected from a rotamer library of the NTA-SH tag by the criterion of producing the best $\Delta\chi$-tensor fit. This fit of a single $\Delta\chi$ tensor to the 3D structure and the experimental PCSs determined the position of the metal ion. The side-chain dihedral angles of the aspartate and glutamate residues were subsequently adjusted manually to bring the carboxyl group into close proximity of the lanthanide ion without introducing van der Waals clashes. The mutants are **a** E200/C204, **b** D200/C204, **c** C204, **d** C200/E204, **e** C200/D204 and **f** C200

NMR spectrometer yielded RDCs ranging from −9.5 to +10.3 Hz, whereas the corresponding measurements with the C200/D204 mutant with IDA-SH tag yielded RDCs ranging from −0.4 to 10.8 Hz (Fig. S7). The largest observed RDC values are thus in good agreement with expectations for immobilized metal ions.

In the case of ERp29-C, we found that the 2.9 Å crystal structure of the human protein (Barak et al. 2009) delivered better $\Delta\chi$-tensor fits than the original NMR structure of the rat protein (Liepinsh et al. 2001). As the human protein shares only 84 % sequence identity with the rat protein and has a one-residue insertion in the loop between helices 4

and 5, we did not expect perfect fits. A reassessment of the 3D structure of the rat protein will be presented elsewhere.

Large-amplitude motions of the metal ion with respect to the protein could thwart a good fit of the PCSs by a single $\Delta\chi$ tensor. Fortunately, the small size of the IDA-SH and NTA-SH tags limits the magnitude of the displacements that the bound metal ion can undergo. Importantly, the present work shows that the lanthanide complexes of either tag can be effectively tied to the protein by aspartate and glutamate residues, and that the effective $\Delta\chi$ tensors obtained produce high-quality fits of the experimental PCSs, as indicated by small Q-factors (Table 2). Thus, while we cannot exclude the possibility of residual tag mobility even in the mutants that produce the largest $\Delta\chi$ tensors, the quality of the fits suggests that the $\Delta\chi$ tensors obtained can be used for reliable predictions of the PCSs of, e.g., ligands binding to the tagged protein. Conversely, the possibility of residual mobility means that the models of Figs. 3 and 5 must not be regarded as the only possible tag conformations.

For best immobilization of a lanthanide ion bound to the NTA-SH tag, it seems to be important that the assisting negatively charged residue is present only in one of the neighboring helix turns. For example, an NTA-SH tag attached to Cys28 of the ubiquitin mutant Ala28Cys has a glutamate in position $i-4$ and an aspartate in position $i+4$ of the α-helix, but only small $\Delta\chi$ values were reported for the Tm^{3+} complex ($\Delta\chi_{ax} = -4.2 \times 10^{-32}$ m^3; Swarbrick et al. 2011b). The presence of Glu24 was not a problem with the IDA-SH tag, as this tag seems partial to an aspartate residue in position $i+4$.

N_z-exchange experiments of the ERp29-C mutant C200/D204 with IDA-SH tag proved to be rather insensitive. To encourage the exchange of metal ions, we performed the experiments with a metal-to-protein ratio of 6:1, using an equimolar mixture of Y^{3+} and Tm^{3+}. The largest exchange peaks were observed for a mixing time of 100 ms, but even under those conditions, only very few exchange peaks could be identified. We feel that, in general, the larger $\Delta\chi$ tensors offered by the NTA-SH tag outweigh the benefit of the IDA-SH tag arising from the possibility to perform exchange experiments.

In conclusion, we recommend using either the IDA-SH tag with an aspartate residue in position $i+4$ or the NTA-SH tag with a glutamate residue in position $i-4$. In both cases, the residues must be located in an α-helix and a competing negatively charged residue in position $i+4$ should be avoided for NTA-SH tags. As α-helices are readily identified by characteristic backbone chemical shifts and their solvent-exposed faces can be predicted by the occurrence of charged residues, we expect that this tagging strategy will prove valuable for a wide range of structural studies, including ligand binding and protein structure determinations.

Acknowledgments We thank Dr. Thomas Huber for generating the rotamer libraries of the IDA-SH and NTA-SH tags. Financial support by the Australian Research Council is gratefully acknowledged.

References

Allegrozzi M, Bertini I, Janik MBL, Lee YM, Liu G, Luchinat C (2000) Lanthanide-induced pseudocontact shifts for solution structure refinements of macromolecules in shells up to 40 Å from the metal ion. J Am Chem Soc 122:4154–4161

Banci L, Bertini I, Cavallaro G, Giachetti A, Luchinat C, Pargi G (2004) Paramagnetism-based restraints for Xplor-NIH. J Biomol NMR 28:249–261

Barak NN, Neumann P, Sevvana M, Schutkowski M, Neumann K, Malesevic M, Reichardt H, Fischer G, Stubbs MT, Ferrari DM (2009) Crystal structure and functional analysis of the protein disulfide isomerase-related protein ERp29. J Mol Biol 385: 1630–1642

Barthelmes K, Reynolds AM, Peisach E, Jonker HRA, DeNunzio NJ, Allen KN, Imperiali B, Schwalbe H (2011) Engineering encodable lanthanide-binding tags into loop regions of proteins. J Am Chem Soc 133:808–819

Bertini I, Luchinat C, Parigi G (2002) Magnetic susceptibility in paramagnetic NMR. Prog Nucl Magn Reson Spectr 40:249–273

de la Cruz L, Nguyen THD, Ozawa K, Shin J, Graham B, Huber T, Otting G (2011) Binding of low-molecular weight inhibitors promotes large conformational changes in the dengue virus NS2B-NS3 protease: fold analysis by pseudocontact shifts. J Am Chem Soc 133:19205–19215

DeLano WL (2002) The PyMOL molecular graphics system. Palo Alto, CA

Dvoretsky A, Gaponenko V, Rosevear PR (2002) Derivation of structural restraints using a thiol-reactive chelator. FEBS Lett 528:189–192

Graham B, Loh CT, Swarbrick JD, Ung P, Shin J, Yagi H, Jia X, Chhabra S, Balow N, Pintacuda G, Huber T, Otting G (2011) DOTA-amide lanthanide tag for reliable generation of pseudocontact shifts in protein NMR spectra. Bioconj Chem 22: 2118–2125

Häussinger D, Huang J, Grzesiek S (2009) DOTA-M8: an extremely rigid, high-affinity lanthanide chelating tag for PCS NMR spectroscopy. J Am Chem Soc 131:14761–14767

Ikegami T, Verdier L, Sakhaii P, Grimme S, Pescatore B, Saxena K, Fiebig KM, Griesinger C (2004) Novel techniques for weak alignment of proteins in solution using chemical tags coordinating lanthanide ions. J Biomol NMR 29:339–349

Jia X, Maleckis A, Huber T, Otting G (2011) 4, 4′-dithiobisdipicolinic acid: a small and convenient lanthanide binding tag for protein NMR spectroscopy. Chem Eur J 17:6830–6836

John M, Park AY, Pintacuda G, Dixon NE, Otting G (2005) Weak alignment of paramagnetic proteins warrants correction for residual CSA effects in measurements of pseudocontact shifts. J Am Chem Soc 127:17190–17191

John M, Pintacuda G, Park AY, Dixon NE, Otting G (2006) Structure determination of protein-ligand complexes by transferred paramagnetic shifts. J Am Chem Soc 128:12910–12916

John M, Headlam MJ, Dixon NE, Otting G (2007) Assignment of paramagnetic ^{15}N-HSQC spectra by heteronuclear exchange spectroscopy. J Biomol NMR 37:43–51

Keizers PH, Desreux JF, Overhand M, Ubbink M (2007) Increased paramagnetic effect of a lanthanide protein probe by two-point attachment. J Am Chem Soc 129:9292–9293

Keizers PH, Saragliadis A, Hiruma Y, Overhand M, Ubbink M (2008) Design, synthesis, and evaluation of a lanthanide chelating protein probe: cLaNP-5 yields predictable paramagnetic effects independent of environment. J Am Chem Soc 130:14802–14812

Keizers PH, Mersinli B, Reinle W, Donauer J, Hiruma Y, Hannemann F, Overhand M, Bernhardt R, Ubbink M (2010) A solution model of the complex formed by adrenodoxin and adrenodoxin reductase determined by paramagnetic NMR spectroscopy. Biochemistry 49:6846–6855

Knight MJ, Pell AJ, Bertini I, Felli C, Gonnelli L, Pierattelli R, Herrmann T, Emsley L, Pintacuda G (2012) Structure and backbone dynamics of a microcrystalline metalloprotein by solid-state NMR. Proc Natl Acad Sci 109:11095–11100

Koehler J, Meiler J (2011) Expanding the utility of NMR restraints with paramagnetic compounds: background and practical aspects. Prog Nucl Magn Reson Spectr 59:360–389

Kramer F, Deshmukh MV, Kessler H, Glaser SJ (2004) Residual dipolar coupling constants: an elementary derivation of key equations. Concepts Magn Reson 21A:10–21

Li QF, Yang Y, Maleckis A, Otting G, Su XC (2012) Thiol-ene reaction: a versatile tool in site-specific labelling of proteins with chemically inert tags for paramagnetic NMR. Chem Commun 48:2704–2706

Liepinsh E, Baryshev M, Sharipo A, Ingelman-Sundberg M, Otting G, Mkrtchian S (2001) Thioredoxin-fold as a homodimerization module in the putative chaperone ERp29: nMR structures of the domains and experimental model of the 51 kDa homodimer. Structure 9:457–471

Liu WM, Keizers PH, Hass MA, Blok A, Timmer M, Sarris AJ, Overhand M, Ubbink M (2012) A pH-sensitive, colorful, lanthanide-chelating paramagnetic NMR probe. J Am Chem Soc 134:17306–17313

Ma C, Opella SJ (2000) lanthanide ions bind specifically to added "EF-hand" and orient a membrane protein in micelles for solution NMR spectroscopy. J Magn Reson 146:381–384

Man B, Su XC, Liang H, Simonsen S, Huber T, Messerle B, Otting G (2010) 3-Mercapto-2, 6-pyridinedicarboxylic acid, a small lanthanide-binding tag for protein studies by NMR spectroscopy. Chem Eur J 16:3827–3832

Martin LJ, Hähnke MJ, Nitz M, Wöhnert J, Silvaggi NR, Allen KN, Schwalbe H, Imperiali B (2007) Double-lanthanide-binding tags: design, photophysical properties, and NMR applications. J Am Chem Soc 129:7106–7113

Neylon C, Brown SE, Kralicek AV, Miles CS, Love CA, Dixon NE (2000) Interaction of the *Escherichia coli* replication terminator protein (Tus) with DNA: a model derived from DNA-binding studies of mutant proteins by surface plasmon resonance. Biochemistry 39:11989–11999

Otting G (2008) Prospects for lanthanides in structural biology by NMR. J Biomol NMR 42:1–9

Otting G (2010) Protein NMR using paramagnetic ions. Annu Rev Biophys 39:387–405

Peters F, Maestre-Martinez M, Leonov A, Kovačič L, Becker S, Boelens R, Griesinger C (2011) Cys-Ph-TAHA: a lanthanide binding tag for RDC and PCS enhanced protein NMR. J Biomol NMR 51:329–337

Pintacuda G, Park AY, Keniry MA, Dixon NE, Otting G (2006) Lanthanide labeling offers fast NMR approach to 3D structure determination of protein–protein complexes. J Am Chem Soc 128:3696–3702

Pintacuda G, John M, Su XC, Otting G (2007) NMR structure determination of protein-ligand complexes by lanthanide labelling. Acc Chem Res 40:206–212

Prudêncio M, Rohovec J, Peters JA, Tocheva E, Boulanger MJ, Murphy MEP, Hupkes HK, Kosters W, Impagliazzo A, Ubbink M (2004) A caged lanthanide complex as a paramagnetic shift agent for protein NMR. Chem Eur J 10:3252–3260

Rodriguez-Castañeda F, Haberz P, Leonov A, Griesinger C (2006) Paramagnetic tagging of diamagnetic proteins for solution NMR. Magn Reson Chem 44:S10–S16

Saio T, Ogura K, Yokochi M, Kobashigawa Y, Inagaki F (2009) Two-point anchoring of a lanthanide-binding peptide to a target protein enhances the paramagnetic anisotropic effect. J Biomol NMR 44:157–166

Saio T, Yokochi M, Kumeta H, Inagaki F (2010) PCS-based structure determination of protein–protein complexes. J Biomol NMR 46:271–280

Saio T, Ogura K, Shimizu K, Yokochi M, Burke TR Jr, Inagaki F (2011) An NMR strategy for fragment-based ligand screening utilizing a paramagnetic lanthanide probe. J Biomol NMR 51: 395–408

Schmitz C, Park AY, Dixon NE, Otting G, Pintacuda G, Huber T (2006) Efficient χ-tensor determination and NH assignment of paramagnetic proteins. J Biomol NMR 35:79–87

Schmitz C, Stanton-Cook MJ, Su XC, Otting G, Huber T (2008) Numbat: an interactive software tool for fitting $\Delta\chi$-tensors to molecular coordinates using pseudocontact shifts. J Biomol NMR 41:179–189

Schmitz C, Vernon R, Otting G, Baker D, Huber T (2012) Protein structure determination from pseudocontact shifts using ROSETTA. J Mol Biol 416:668–677

Su XC, Otting G (2010) Paramagnetic labelling of proteins and oligonucleotides for NMR. J Biomol NMR 46:101–112

Su XC, Huber T, Dixon NE, Otting G (2006) Site-specific labelling of proteins with a rigid lanthanide-binding tag. Chem BioChem 7:1599–1604

Su XC, Man B, Beeren S, Liang H, Simonsen S, Schmitz C, Huber T, Messerle B, Otting G (2008) A dipicolinic acid tag for rigid lanthanide tagging of proteins and paramagnetic NMR spectroscopy. J Am Chem Soc 130:10486–10487

Su XC, Liang H, Loscha KV, Otting G (2009) $[Ln(DPA)_3]^{3-}$ is a convenient paramagnetic shift reagent for protein NMR studies. J Am Chem Soc 131:10352–10353

Swarbrick JD, Ung P, Chhabra S, Graham B (2011a) An iminodiacetic acid based lanthanide binding tag for paramagnetic exchange NMR spectroscopy. Angew Chem Int Ed 50:4403–4406

Swarbrick JD, Ung P, Su XC, Maleckis A, Chhabra S, Huber T, Otting G, Graham B (2011b) Engineering of a bis-chelator motif into a protein α-helix for rigid lanthanide binding and paramagnetic NMR spectroscopy. Chem Commun 47:7368–7370

Vlasie MD, Comuzzi C, van den Nieuwendijk AM, Prudêncio M, Overhand M, Ubbink M (2007) Long-range-distance NMR effects in a protein labeled with a lanthanide-DOTA chelate. Chemistry 13:1715–1723

Wöhnert J, Franz KJ, Nitz M, Imperiali B, Schwalbe H (2003) Protein alignment by a coexpressed lanthanide-binding tag for the measurement of residual dipolar couplings. J Am Chem Soc 125: 13338–13339